Direct 3D Ultrasound to Video Registration Using Photoacoustic Effect

Alexis Cheng, Jin U. Kang, Russell H. Taylor, and Emad M. Boctor

The Johns Hopkins University, Baltimore, Maryland 21211, United States of America
{acheng22,jkang,rht}@jhu.edu, eboctor1@jhmi.edu

Abstract. Interventional guidance systems require surgical navigation systems to register different tools and devices together. Standard navigation systems have various drawbacks leading to target registration errors (TRE) of around 3mm. The aim of this work is to introduce the photoacoustic (PA) effect as a direct 3D ultrasound (US) to video registration method. We present our experimental setup and demonstrate its feasibility on both a synthetic phantom and an *ex vivo* tissue phantom. We achieve an average TRE of 560 microns and standard deviation of 280 microns on a synthetic phantom. Also, an average TRE of 420 microns and standard deviation of 150 microns on the *ex vivo* tissue phantom are obtained. We describe a roadmap to bring this system into the surgical setting and highlight possible challenges along the way.

Keywords: Instrument & Patient Localization and Tracking, Registration, Planning and image guidance of interventions, Visualization, Abdominal imaging, Oncology Applications, Optical imaging, Ultrasound.

1 Introduction

Interventional guidance systems are commonly used in modern surgical procedures, including open surgery, laparoscopic surgery, and robotic surgery [1]. The guidance systems are used because it is often difficult to locate tumors both due to its movement during the procedure and the camera's limited field of view. Guidance systems typically provide a fusion of video and other imaging modalities to reduce the difficulty in locating regions of interest. Before they can be used, these guidance systems must be registered with a number of surgical tools and devices. To accomplish this registration, several guidance systems are equipped with electromagnetic (EM) or optical surgical navigation systems [2], [3].

Stolka et al. [3] present an EM-based laparoscopic intra-operative ultrasound navigation system similar to standard EM-based systems shown in Figure 1A. These systems typically have several drawbacks including the number of EM sensors that must be placed on all tools in order to be tracked by the navigation system and the need to indirectly transform from one coordinate frame to another. An indirect transformation is defined to be one where the transformation to the coordinate frame of interest cannot be obtained without computing a chain of transformations via intermediate coordinate

N. Ayache et al. (Eds.): MICCAI 2012, Part II, LNCS 7511, pp. 552–559, 2012.

frames. As an example, to obtain the transformation from EM space to the US image space, the transformation from the EM frame to the marker on the US probe and the transformation from the marker to the US frame are needed. Determining this second transformation presents another problem of calibration. A number of authors [4], [5] have presented research on specific calibration processes, attempting to minimize the error. Typically, they have demonstrated errors of around 3mm [4], [6], [7].

Yip et al. [8] have demonstrated a registration method that utilizes a tool serving as both fiducials in the US space and markers in the stereo camera (SC) space. Some drawbacks for this system include the need to have a custom registration tool touching the surface and the segmentation of fiducials from noisy US images.

Vyas et al. [9] demonstrated proof of concept for a direct registration method with the PA effect. For this paper, a direct registration method is defined to be one that only requires a single transformation between frames as opposed to a chain of transformations. The method addresses each of the drawbacks above. A marker is not necessary to generate a coordinate transformation between the tracker frame and the US transducer frame. Previous work [10], [11] shows that a pulsed laser source can effectively generate the photoacoustic (PA) signal in tissue, resulting in an acoustic wave that can be detected by conventional US transducers [12], [13]. Other than the US transducer, nothing else needs to touch the surface. Each laser point projection can be seen as a green spot in the SC space and as a PA signal in the US space. Segmentation of the PA signal is also simpler in a PA image because the laser spot is the only acoustic source. Finally, the calibration process is unnecessary since the coordinate transformation from the SC frame to the US frame can be computed directly with the two 3D point sets based on rigid registration algorithms [2], [16].

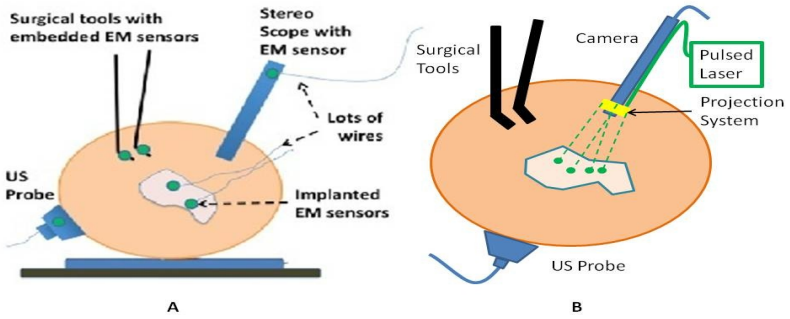

Fig. 1. A) Standard EM-based Navigation System, B) PA Navigation System

Our work introduces the PA effect and PA imaging as a new medical tracking technology and is a step towards realizing the system shown in Figure 1B. We aim to present a direct 3D US to video registration method and to demonstrate its feasibility on *ex vivo* tissue. Improving on [9], we use a 3D US transducer instead of a 2D US transducer to detect the PA signal. Using a 3D transducer allows this registration method to function for a non-planar set of 3D points. This is a significant advantage because we aim to deploy this method in a laparoscopic environment and organ surfaces will rarely form a planar surface. We also improve significantly on the point

finding algorithms used in [9] for both SC images and US volumes. In addition to using a synthetic phantom with excellent light absorption characteristics, we also use a piece of resected *ex vivo* porcine liver tissue embedded in a gelatin phantom to demonstrate this method's feasibility in a practical environment and eventual deployment in our intended applications of laparoscopic tumor resections.

This paper will detail the experimental procedure and algorithms to validate this method on a synthetic phantom and an *ex vivo* liver phantom using a 3D US transducer. We will present target registration error (TRE) results. Possible challenges in bringing this system into the surgical setting will also be discussed.

2 Methods

To perform our experiment, we use a Q-switched neodymium-doped yttrium aluminum garnet (Nd:YAG), Brilliant (Quantel Laser, France) laser frequency doubled to 532nm wavelength at approximately 6mJ/cm^2 to generate a PA effect on the synthetic phantom and approximately 19mJ/cm^2 on the *ex vivo* tissue phantom. At this wavelength, most of the laser energy is absorbed at the superficial surface of the tissue. However, there is slight penetration into the tissue, creating a source of error that will be discussed. Our stated energy is lower than the maximum permissible exposure of 19.5mJ/cm^2 as calculated from the IEC 60825-1 laser safety standard [14] based on a 0.25s exposure time, a 4ns pulse width, and a frequency of 10Hz. Alternate tests showed that a lower energy was also able to generate a PA effect on *ex vivo* tissue. We use a SonixCEP US system along with a 4DL14-5/38 US transducer developed by Ultrasonix Medical Corporation (Richmond, Canada) to scan the volume of interest. The motor actuation of this transducer induces angular movement around an internal pivot point. The Sonix DAQ device, developed in collaboration between the University of Hong Kong and Ultrasonix, and the MUSiiC toolkit [15] is used to acquire pre-beamformed radiofrequency (RF) data directly from the US machine. We use the k-wave toolbox [16] in MATLAB (Mathworks Inc. Natick, MA) designed for reconstructing PA images based on RF data. A custom-built SC system containing two CMLN-13S2C cameras (Point Grey Research, Richmond, Canada) is used to capture images to be used for 3D triangulation. The synthetic phantom is made using plastisol and black dye. The *ex vivo* liver phantom is made using a gelatin solution and a freshly resected porcine liver. The surface of the liver is partially exposed and not covered by gelatin. Alternate tests with other surfaces such as porcine kidney tissue and fat were also successful in generating a PA signal.

Our experiment can be split into a data collection phase and a data processing phase. The data collection phase outputs SC image pairs, five frames for each camera, and a 3D RF US volume for each projected laser spot. The number of frames is arbitrary. The data processing phase uses the data and generates a coordinate transformation from the SC frame to the US frame. Figure 2A shows the experimental setup and an overlay of a US image representation using the inverse of the transformation.

Figure 3A shows the workflow of the data collection phase. First a laser spot is projected onto the exposed surface of the *ex vivo* liver phantom. There will be inaccuracies

in SC spot triangulation if the laser spot is projected at or near the liver gelatin interface because the laser spots become irregularly shaped when projected onto clear materials. Second, several images are taken for each camera. The laser spot projected onto the phantom must be visible in at least one image per camera for triangulation to be possible. Our cameras have a faster capture rate than our laser's repetition rate, so some of the frames will be devoid of the laser signal. We will exploit this during data processing. Steps 3 and 4 show that the 3D US transducer motor actuation and RF data are intermittently collected from the DAQ device to scan and acquire the RF data of the volume of interest. The volume's field of view is 14.7° for the *ex vivo* tissue phantom, 19.6 ° for the synthetic phantom and the motor step size is 0.49°. This iterative process is manual, but an automatic process is in development. This workflow is repeated for each of the thirty laser spots.

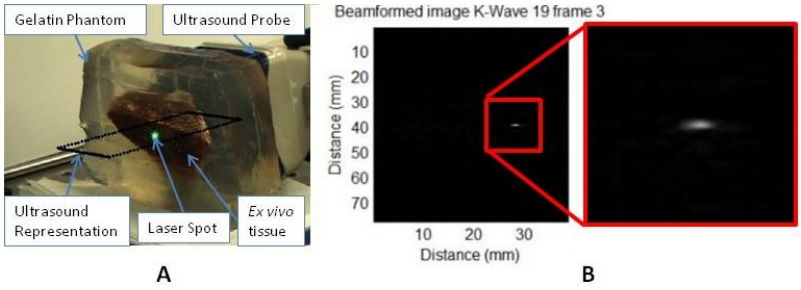

Fig. 2. A) Experimental Setup and Video Overlay, B) PA Signal within an US image

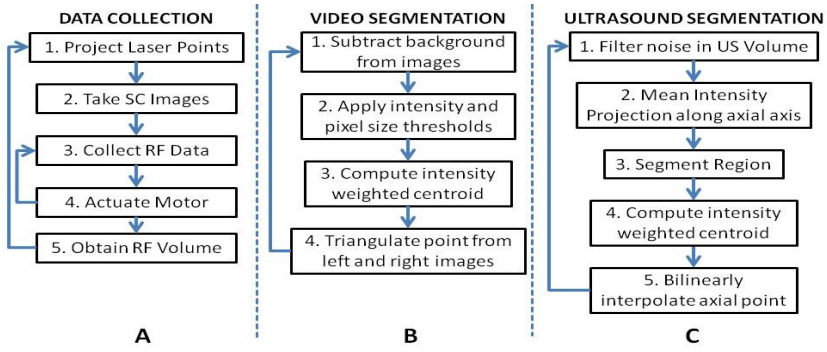

Fig. 3. Workflow for A) Data Collection, B) SC Segmentation, and C) US Segmentation

The data processing phase involves the segmentation of the SC images into 3D SC points, the segmentation of the 3D RF US volume data into 3D US points, and the computation of the transformation from the SC frame to the US frame.

Figure 3B shows the workflow for SC segmentation. For each camera, we pick a SC image with the laser spot and without the laser spot. Next, the background images without the laser spot are subtracted from the images with the laser spot. This step makes it significantly easier to segment the laser spot. We then apply an appropriate intensity and pixel size thresholds such that the laser spot is segmented out.

These thresholds are selected based on the laser beam diameter and the phantom's reflectance. Next, we fit an ellipse to the segmented region and compute the intensity weighted centroid. Calibration files for our specific SC allow us to triangulate the segmented point from each camera and obtain a single 3D point in the SC frame. This workflow is repeated for each laser spot projection. We use thirty sets of SC images.

The workflow for the segmentation of the 3D RF US volume is shown in Figure 3C. First, for each slice of a 3D RF US volume, the RF data is beamformed using the k-wave toolbox [16] in MATLAB. The dynamic range of the image is normalized with respect to the volume to decrease the size of the PA signal seen in each volume. Figure 2B shows the the k-wave beamformed PA signal image. Next, we project the volume onto the lateral-elevational plane by taking the mean along each axial ray. An appropriate intensity and pixel size threshold is then applied to this image. An ellipse is fitted on the segmented region and an intensity-weighted centroid is computed resulting in lateral and elevational coordinates. As described earlier, the PA signal originates from the surface and any penetration into the surface. Since air cannot generate a PA signal in our setup, we can exploit that the high intensity pixels farthest away in the axial direction are from the surface. Thus, we obtain the axial coordinate corresponding with a lateral-elevational coordinate as the axial-most high intensity pixel. This step is particularly important because the penetration of the laser pulse is much deeper for the *ex vivo* tissue phantom than the penetration for the synthetic phantom. We use bilinear interpolation to obtain axial coordinates between sampled points. These three coordinates are converted to 3D US coordinates based on transducer specifications. This workflow is repeated for each of our thirty 3D RF US volumes.

The transformation from the SC frame to the US frame can be computed with the 3D SC and 3D US point sets. Any registration method for computing the transformation between two 3D point sets can be used. We use the coherent point drift algorithm [17] in our experiment. One of the main reasons for using coherent point drift is that it allows for data points to be missing from either dataset. An assumption that we have made is that each laser spot will be visible in the SC images and each PA signal will be visible in the US volume. This assumption is valid for our experiment, but may not hold in the surgical setting due to SC or transducer movement. The coherent point drift registration algorithm allows us to acquire a registration as long as there are enough corresponding points in the SC images and the US volume.

The transformation from the SC frame to the US frame is used to transform the 3D SC points to the US frame for validation. The inverse transformation is used to display a representation of an US image into the SC frame as shown in Figure 2A.

3 Results

The results of our experiment on the synthetic phantom and on the *ex vivo* tissue phantom are validated using the target registration error (TRE) metric defined in equation 1. F_{SC_US} is the transformation from the SC frame to the US frame and is computed with all of SC and US points except for one. The TRE is the resulting difference between the actual US test point and the transformed SC test point in the US frame.

$$\overrightarrow{TRE} = \boldsymbol{F_{SC\_US}} * \overrightarrow{SC_{test}} - \overrightarrow{US_{test}} \quad (1)$$

Twenty-nine of the thirty points are used to compute the transformation from the SC frame to the US frame. The remaining point is used as a test point to compute the TRE. This computation is repeated with each of the thirty points as test points. Table 1 shows the average and standard deviation of the TRE results for the thirty cases in the synthetic phantom and the *ex vivo* tissue phantom experiment respectively.

Table 1. Average TRE Results for Leave One Out Registration Experiments

n = 30	Synthetic Phantom	*Ex vivo* Tissue Phantom
Lateral (mm)	0.21 ± 0.17	0.22 ± 0.16
Axial (mm)	0.21 ± 0.13	0.24 ± 0.15
Elevational (mm)	0.41 ± 0.31	0.18 ± 0.10
Euclidean Norm (mm)	0.56 ± 0.28	0.42 ± 0.15

4 Discussion

There are several considerations when discussing this system's deployment in our intended applications of laparoscopic tumor resections. The first is the placement of the transducer. In our experiments, we use a relatively large 3D US transducer that would be near impossible to put inside the body during a laparoscopic procedure. However, the transducer is often placed externally [3], [8] in these procedures, so the size of the probe is not an issue. Naturally, there are disadvantages of placing the transducer externally and farther from the region or organ of interest. The quality of ultrasound images degrades as the depth increases, which would likely lead to errors in localizing fiducials or, in our case, the PA signal. However, since the PA signal only has to travel in one direction, as opposed to traditional US, our PA images will have better quality than US images of equivalent depth.

Another issue with our 3D US transducer is the acquisition speed. There are certain applications where an acquisition speed of a volume per several seconds is sufficient, but a real-time implementation would require a higher acquisition rate. We anticipate using 2D array US transducers for a real-time implementation. These transducers would provide an acquisition rate on the order of twenty volumes per second. The 2D array transducer could also be miniaturized and placed closer to the region of interest.

A third issue deals with the laser delivery system. As shown in our experimental setup, a laser would have to be fired at the organ in free space. This occurrence is unlikely in practical situations. We are developing a fiber delivery tool that will allow us to safely guide the laser beam into the patient's body. This tool will also be able to project concurrent laser spots, greatly enhancing our registration acquisition rate.

At the level of error measurements shown in table 1, it is likely that the calibration of the SC system is a significant contributor. They are able to locate point sources at sub-millimeter accuracy [6], [7]. This error is usually negligible in comparison with the 3mm errors from calibration. Since our results are 0.56mm and 0.42mm errors

respectively, the SC system's error becomes significant. We use a custom SC system, so its errors are likely greater than a finely tuned commercial SC system.

The experimental results in table 1 show that our system achieves sub-millimeter TRE measurements for both the synthetic phantom and the *ex vivo* tissue phantom. There is a slight difference in the results, and it is entirely due to the elevational error. This is likely due to the larger field of view in the synthetic phantom experiment as well as normal variation across experiments. More experiments must be performed to obtain an average error across multiple experiments.

There are a couple of factors that will affect these errors as we move from a bench-top setup to *in vivo* experiments. When our SC system is replaced with a stereo endoscopic camera, the errors may increase. This is because our SC system has a larger disparity than standard stereo endoscopic cameras. Further work will be done to quantify the effects of this change. Also, the errors are reported based on surface points. Since the region of interest is often subsurface, our reported TRE will be biased for subsurface target errors. We believe that the bias will be fairly small since the PA spots are being detected in the same modality as any subsurface regions.

5 Conclusion

We have proposed an innovative 3D US to video direct registration medical tracking technology based on the PA effect and demonstrated its feasibility on an *ex vivo* tissue phantom. The results have been shown to have higher accuracy than state of the art surgical navigation systems. Future work will include the development of a fiber delivery tool, spot finding algorithms to support concurrent spot projection, and subsequent *in vivo* animal experiments. Integration of this direct registration method into laparoscopic or robotic surgery environments will also be a point of emphasis.

Acknowledgements. Financial support for this project was provided by Johns Hopkins University internal funds and NSF grant IIS-1162095. The authors wish to thank Xiaoyu Guo for the optical setup, Hyun-Jae Kang and Nathanael Kuo for help with the MUSiiC toolkit, and Daniel Carnegie for help with *ex vivo* phantoms.

References

1. Wang, Y., Butner, S., Darzi, A.: The developing market for medical robotics. Proceedings of the IEEE 94(9), 1763–1771 (2006)
2. Taylor, R., Lavallee, S., Burdea, G., Mosges, R.: Computer integrated surgery. MIT Press, Cambridge (1996)
3. Stolka, P.J., Keil, M., Sakas, G., McVeigh, E., Allaf, M.E., Taylor, R.H., Boctor, E.M.: A 3D-elastography-guided system for laparoscopic partial nephrectomies. In: Medical Imaging 2010: Visualization, Image-Guided Procedures, and Modeling, San Diego, February 13-18, vol. 76251I, p. 76251I-12 (2010)

4. Boctor, E., Viswanathan, A., Choti, M., Taylor, R., Fichtinger, G., Hager, G.: A Novel Closed Form Solution for Ultrasound Calibration. In: International Symposium on Biomedical Imaging, Arlington, pp. 527–530 (2004)
5. Poon, T., Rohling, R.: Comparison of calibration methods for spatial tracking of a 3-D ultrasound probe. Ultrasound in Medicine and Biology 31(8), 1095–1108 (2005)
6. Navab, N., Mitschke, M., Schuetz, O.: Camera-Augmented Mobile C-arm (CAMC) Application: 3D Reconstruction Using a Low-Cost Mobile C-arm. In: Taylor, C., Colchester, A. (eds.) MICCAI 1999. LNCS, vol. 1679, pp. 688–697. Springer, Heidelberg (1999)
7. Wiles, A., Thompson, D., Frantz, D.: Accuracy assessment and interpretation for optical tracking systems. In: Proceedings of SPIE, vol. 5367, pp. 421–432 (2004)
8. Yip, M.C., Adebar, T.K., Rohling, R., Salcudean, S.E., Nguan, C.Y.: 3D Ultrasound to Stereoscopic Camera Registration through an Air-Tissue Boundary. In: Jiang, T., Navab, N., Pluim, J.P.W., Viergever, M.A. (eds.) MICCAI 2010, Part II. LNCS, vol. 6362, pp. 626–634. Springer, Heidelberg (2010)
9. Vyas, S., Su, S., Kim, R., Kuo, N., Taylor, R.H., Kang, J.U., Boctor, E.M.: Interoperative Ultrasound to Stereocamera Registration using Interventional Photoacoustic Imaging. In: Medical Imaging 2012: Visualization, Image-Guided Procedures, and Modeling, San Diego, February 4-9, vol. 8316, p. 83160S (2012)
10. Kolkman, R., Steenbergen, W., van Leeuwen, T.: In vivo photoacoustic imaging of blood vessels with a pulsed laser diode. Lasers in Medical Science 21(3), 134–139 (2006)
11. Kuo, N., Kang, H.J., DeJournett, T., Spicer, J., Boctor, E.M.: Photoacoustic imaging of prostate brachytherapy seeds in ex vivo prostate. In: Medical Imaging 2011: Visualization, Image-Guided Procedures, and Modeling, Lake Buena Vista, February 12-17, vol. 7964, p. 796409 (2011)
12. Xu, M., Wang, L.: Photoacoustic imaging in biomedicine. Review of Scientific Instruments 77, 041101 (2006)
13. Hoelen, C., De Mul, F., Pongers, R., Dekker, A.: Three-dimensional photoacoustic imaging of blood vessels in tissue. Optics Letters 23(8), 648–650 (1998)
14. IEC 60825-1:1993+A1:1997+A2:2001: Safety of Laser Products – Part 1: Equipment Classification and Requirements. International Electrotechnical Commission, Geneva (2001)
15. Kang, H.J., Kuo, N., Guo, X., Song, D., Kang, J.U., Boctor, E.M.: Software framework of a real-time pre-beamformed RF data acquisition of an ultrasound research scanner. In: Medical Imaging 2012: Visualization, February 4-9, vol. 8320, p. 83201 (2012)
16. Treeby, B., Cox, B.: k-Wave: MATLAB toolbox for the simulation and reconstruction of photoacoustic wave-fields. Journalof Biomedical Optics 15(2), 21314 (2010)
17. Myronenko, A., Song, X.: Point-Set Registration: Coherent Point Drift. IEEE Trans. on Pattern Analysis and Machine Intelligence 32(12), 2262–2275 (2010)